5-2017

Modulating Intra-Nuclear LC3 with Small Molecules Rescues Cells from an Aneuploidogen-Induced Phenotype

Daniel P. Rosenberg
College of William and Mary

Modulating Intra-Nuclear LC3 with Small Molecules Rescues Cells from an Aneuploidogen-Induced Phenotype

A thesis submitted in partial fulfillment of the requirement
for the degree of Bachelors of Science in Biology
from The College of William and Mary

by

Daniel Rosenberg

Accepted for: _____
(Honors)

_____
William Buchser

_____
Lizabeth Allison

_____
Lisa Landino

_____
Helen Murphy

Williamsburg, VA
May 4, 2017

Acknowledgements

I would like to thank William Buchser for his guidance and mentorship during the completion of this project, Lizabeth Allison for her support and help in this project in addition to serving on my Honors Committee, alongside Lisa Landino and Helen Murphy.

I would further like to thank everyone who provided assistance in the lab and while writing, including Likhitha Kolla, David Heo, Emily Cassio, Matthew Veenstra, Sara Barlow, Ana Maximova, Cyril Anyetei-Anum, Jibo 'Dylan' Zhang, and Nazila Shafagati.

Author
Daniel Rosenberg
dprosenberg@email.wm.edu

Advisor:
William J Buchser
Department of Biology, College of William & Mary
540 Landrum Dr.
Williamsburg, VA USA
Phone 757-221-1994, Fax 757-221-6483
wjbuchser@wm.edu

Abstract

Nuclear autophagy (nucleophagy) has been described as a cellular metabolic response by which nuclear material is actively degraded after stressors, such as nuclear damage or the onset of tumorigenesis. Here we describe nucleophagy as a process distinct from traditional macroautophagy in human cell lines. We found that although nuclear localization of LC3 is not dependent on particular nuclear importins, knockdown of nuclear importins (causing nuclear stress) can induce a nuclear autophagic response. Our characterization of nucleophagy was facilitated by chemical modulation of the process via two compounds discovered previously in a high content analysis. These small molecules bidirectionally regulate nuclear autophagy in human renal, pancreatic, and bladder cell lines. One molecule (NSC31762 or *DTEP*) *enhances* nuclear autophagic puncta and increases lysosomal targeting of LC3. Another molecule (NSC279895 or *DIHI*) *reduces* the nuclear localization of LC3. Finally, we applied these chemical tools in the setting of aneuploidy driven nuclear stress. The compound DIHI, shown to reduce nuclear autophagic puncta, was able to revert cells from aneuploidogen-induced phenotypes, possibly restoring homeostasis. These new tools will allow for a deeper exploration of nucleophagy, and could serve as proof-of-principle in guiding new therapies for diseases involving nuclear stress.

Keywords
Nucleophagy, Nuclear Autophagy, Cancer, Chemical Screen, LC3, Aneuploidy, Nuclear Import

Table of Contents

Experiment Contributions

Author contributions to each figure listed below. Significant contributions by other researchers listed in parentheses.

Figure 1: Conception, design

Figure 2: Conception, design

Figure 3: Conception, acquisition, analysis (David Heo, Emily Cassio, Likhitha Kolla)

Figure 4: Conception, analysis (David Heo, Emily Cassio, Likhitha Kolla)

Figure 5: Conception, acquisition, design, analysis

Figure 6: Conception, acquisition, design, analysis

Figure 7: Acquisition, analysis (Matthew Veenstra, Dylan Zhang)

Figure 8: Analysis (Likhitha Kolla)

Figure 9: Acquisition, analysis (Likhitha Kolla)

Introduction

Macroautophagy: The Cell's Recycling System

Autophagy is the systematic recycling and destruction of cellular components, such as ineffectual organelles, and is a basal process in nearly all eukaryotes (Levine and Klionsky). Evolved as an adaptation of eukaryotic cells to survive during starvation conditions, autophagy allows for nutrients otherwise inaccessible within the cell to be sacrificed for survival (Rogov et al.). Research in the 1960's hinted at an early mechanism for membrane recycling in the lysosome with an emphasis on substrate specificity (Yang and Klionsky). It wasn't until the 1990's that molecular biology techniques and theories were applied in the setting of autophagy, resulting in the rapid expansion of autophagy research and the culmination in the 2016 Nobel Prize in Physiology or Medicine. Work in the Ohsumi lab revealed morphological similarities between mammals and yeast, ultimately elucidating the first autophagy gene *ATG1* through genetic screens of yeast mutants (Tsuboi). Macroautophagy is traditionally considered to be a nonselective process; an overview of the steps of macroautophagy are provided in **Figure 1**. Recent specific forms of selective autophagy have been described, however, and each has maintained certain core Atg proteins necessary for the main molecular machinery required for autophagosome formation (Xie and Klionsky). The implication of autophagy as a basal process necessary for development and survival, as well as its role in the progression of many diseases, highlights the need for further research to understand the intricacies of this phenomenon.

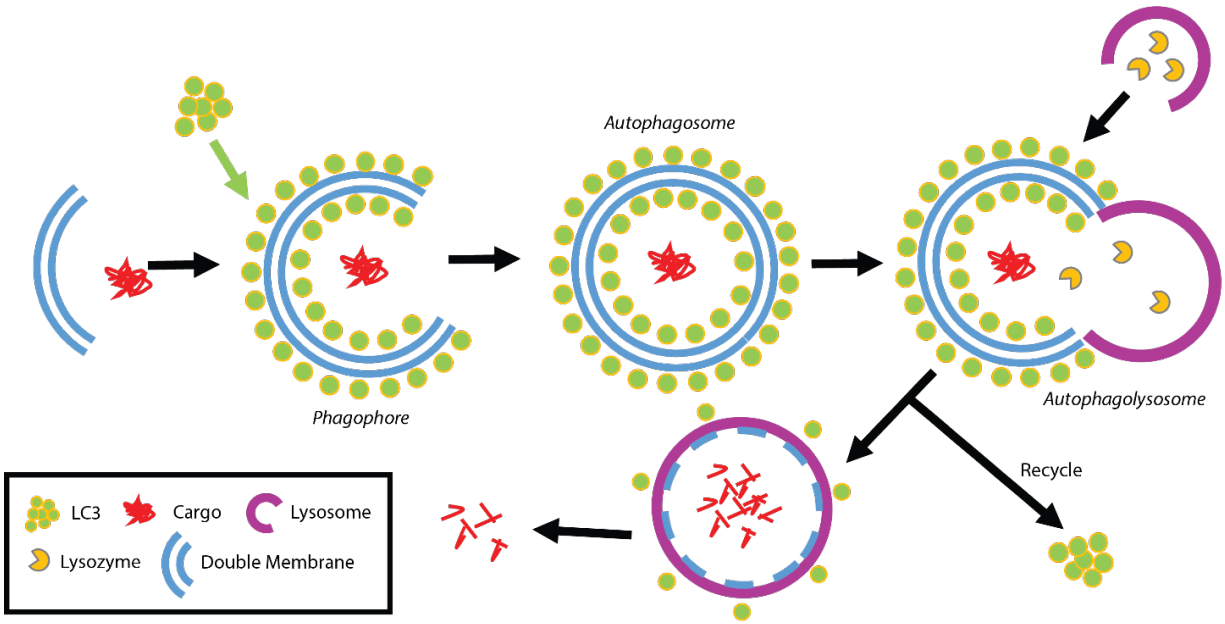

Figure 1. Mechanism of macroautophagy Graphical representation of the general macroautophagy pathway. 'Cargo' (red) is engulfed by a structure called a phagophore initiated by the ULK1/2 complex among other proteins. Proteins, including ATG9 and LC3 (green) help to form the autophagosome, which completely surrounds the cargo. This structure can then either fuse with an endosome (and eventually a lysosome) or a lysosome (purple) directly, forming the autophagosome where hydrolases degrade the cargo and recycle components in the cytosol (Carneiro and Travassos).

Basal autophagy is generally defined as a homeostasis mechanism and the primary source of essential nutrients, where *induced* autophagy is not necessarily present; this is under normal conditions and short, non-fatal periods of starvation (Mizushima);(Codogno and Meijer). Particularly in the brain, autophagy may be initiated to counteract the detrimental effects of starvation and hypoxia, converting amino acid energy into essential glucose to fuel critical tissues and erythrocytes (Codogno and Meijer). Light chain 3 (LC3), a subunit of microtubule-associated protein 1A (MAP1A) and MAP1B, is an invaluable marker of autophagy as it associates with the autophagic machinery upon initiation of autophagy. Alongside yeast proteins Atg8/Apg8/Aut8, these markers are associated with a ubiquitination-like conjugation system which mediate membrane formation (Ugolino et al.). Ubiquitin-like proteins (UBLs) are

recruited by autophagy receptors to the material the cell needs to degrade, resulting in the association and activation of core machinery (Rogov et al.).

Selective Autophagy

Selective forms of autophagy have now been described with high specificity and regulation, and have been found to span cellular compartments such as the mitochondria (mitophagy), the endoplasmic reticulum (ER-phagy), and the peroxisome (pexophagy) (**Figure 2**) (Gomes and Scorrano; Kraft, Reggiori, and Peter; Mizushima). Of recent interest are autophagy pathways that have been infrequently observed but seem to be implicated in a multitude of disease systems. Nucleophagy, or degradation of nuclear material via an autophagic pathway, has been identified as a unique process in yeast and mammalian systems (Mijaljica and Devenish). Recent studies have confirmed the existence of nucleophagy and have correlated it with diverse cellular processes, including epidermal differentiation (Akinduro et al.), senescence after DNA damage (Dou et al.), and the clearing of extra-nuclear DNA alongside accumulated nuclear envelope proteins (Park et al.; Mijaljica, Prescott, and Devenish). However, the set of conditions under which nucleophagy is activated, the identification of the degraded nuclear substrates, and the mechanism of transport of LC3 into the nucleus and export of nuclear materials are still under investigation.

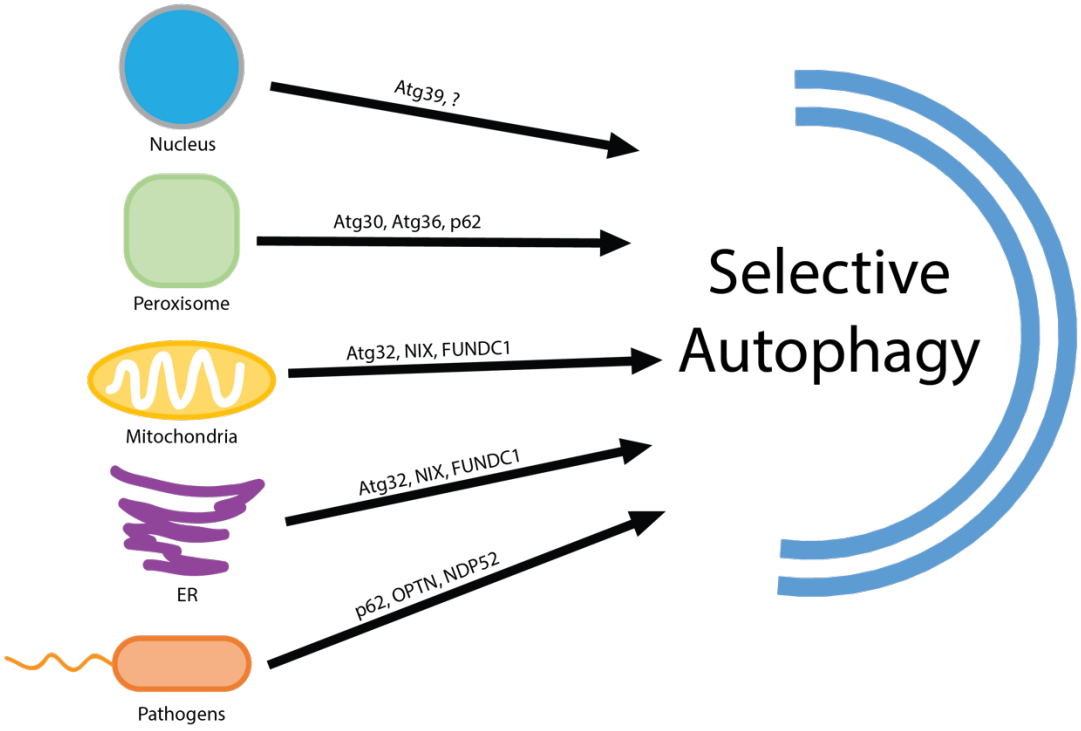

Figure 2. Selective Autophagy Selective autophagy serves to recycle many different components of the cell, including portions of the nucleus (nucleophagy), the peroxisome (pexophagy), mitochondria (mitophagy), endoplasmic reticulum (ER-phagy), pathogens (xenophagy), though this list is not exhaustive. Each is associated with distinct pathways and machinery.

The ER-associated degradation (ERAD) pathway is recognized as the main mechanism by which potentially dangerous, stress-inducing misfolded proteins are mediated. ERAD targets accumulated unfolded proteins, exporting them via a translocon, where they are subsequently degraded by the proteasome. Autophagy is implicated as a means by which substrates can be degraded if the ERAD system is overwhelmed (Yorimitsu et al.). ER-phagy seems to serve as a backup plan for the unfolded protein response, essentially expanding the function of the ER under conditions of high demand (Schuck, Gallagher, and Walter). ER-phagy can be defined as a subset of autophagy, primarily due to a dependence on core autophagy machinery, specifically Atg9 (Lipatova and Segev), as well as the fact that it is ER-specific and is similar to microautophagy, mediated by direct lysosomal engulfment (Yorimitsu et al.). This form of

specific autophagy may provide some insight into the mechanistic differences between nucleophagy and macroautophagy, the details of which are unclear.

Nucleophagy and the Stress Response

Like other forms of autophagy, nucleophagy appears to be a stress response system. It is recognized that the nucleus has complex pathways in place which respond to stress or damage (Mah, El-Osta, and Karagiannis; Kose, Furuta, and Imamoto; Biamonti and Vourc'h). Normally, proteins with a nuclear function enter and exit the nucleus mediated by transporters that are members of the importin/exportin family (Stewart). Disruption of nuclear transport through the nuclear pore complex leads to nuclear stress and subsequent disease phenotypes, including age-related impairments, cancer, and neurodegeneration (Freibaum et al.; D'Angelo et al.; Zhang et al.; Hirano et al.). Here we investigate whether nucleophagy is upregulated in response to nuclear transport stress.

The loss or malfunction of autophagy can lead to cellular damage and the onset of disease (Wong, Cheung, and Ip). When DNA damage occurs in tandem with loss of autophagic function, the result is increased cell death and increased risk of tumorigenesis (Mizushima and Yoshimori). Indeed, it is known that in the setting of tumorigenic stress, selective autophagy may clear damaged DNA, activated oncogenes, and proteotoxic aggregates, stabilizing cancer cells, though the exact mechanisms by which these substrates are recognized remains elusive (Santaguida et al.). Tumors able to survive p53-induced apoptosis exhibit increased levels of autophagy, where cells found at the core of the tumor are protected from necrosis due to nutrient-limited conditions and oncogenic stress (Amaravadi et al.). Macroautophagy has been observed

to aid in cell survival up to weeks after induced nutrient-limiting stress; while survival increases, metabolic upregulation of glycolysis impairs the cell's ability to proliferate (Klionsky et al.).

Autophagy is a critical component of the overall induced stress-response necessary for repair to occur after the onset of disease, inflammation, and the cell's initiation of apoptosis. On a macro level, autophagy has the potential to limit genome damage during tumorigenesis (Mizushima). Bcl-2 proteins, specifically Bcl-2, Bcl-xL, and Mcl-1, are known to be regulators of not just apoptosis, but autophagy as well, as has been observed in Bcl-2 homolog Beclin 1 (Marquez and Xu). Beclin 1 is known to inhibit tumorigenesis and increase autophagy; loss of this gene is implicated in human breast carcinomas (Liang et al.). Treatment of diseases like cancer may be augmented by the inhibition of Blc-2, which would initiate apoptotic pathways. Natural killer (NK) cells are able to induce autophagy both promoting a recovery and repair response while simultaneously potentially promoting the onset and survival of cancer (William J Buchser, Thomas C Laskow).

A more extreme example of a stress phenotype is whole-chromosomal abnormality that changes the numerically standard ploidy of a cell. Cells unable to carry out autophagy exhibit lower survival, yet simultaneously show an increase in mutation rate alongside the induction of aneuploidy (Mathew et al.). Suppression of DNA damage via autophagy may also serve as a tumor suppressant mechanism. It has now been shown that oncogenic mutations and aneuploidy can trigger nucleophagy as a mechanism for the destruction of essential structural proteins (nuclear lamin B1). This ultimately induces cellular senescence and prevents further damage to the organism (Dou et al.). Malignant cancers frequently exhibit aneuploidy (Torres, Williams, and Amon), raising questions as to whether these cells can manipulate autophagy in their favor.

We seek to better understand the interplay between nucleophagy and nuclear stress in the setting of aneuploidy.

Here, we utilize two new chemical modulators to investigate the dynamics of nucleophagy. Given that nuclear autophagic puncta are infrequently observed in untreated cultured cells, these modulators increased their expression allowing for tangible characterization of the process. In this state, the autophagic protein LC3 localizes to regions of the nucleus with low DNA content (nuclear holes), and on occasion with large amounts of extra-nuclear DNA (micronuclei). Our results suggest that nuclear LC3 localization is increased under nuclear stress induced by knockdown of nuclear import proteins. Finally, we use the chemical modulators to investigate the functional role of nucleophagy to mitigate nuclear stress in the setting of aneuploidy.

Methods

High Content Chemical Screening Assay

Medium throughput, high-content screening of 1,600 chemical compounds (NCI DTEP diversity set IV) identified molecules that modulate nucleophagy. 786-0 cells (described below) were cultured on 96-well plates and exposed to either a vehicle (DMSO or PBS) or treatment condition at 10μM. Border wells were excluded to control for well effects. Media was replaced after 4 hours of incubation with the compound, and cells were subject to fixing and staining after 18 hours. Between 2 and 4 biological replicates (discrete passages) were analyzed. Plate layout for the secondary screen is included in **Supplemental Figure 1**.

High content screening (HCS) allowed for automated measurement of biological cellular components using automated microscopy. HCS is commonly used when looking at large numbers of drugs in screenings where cellular activity cannot be measured by a single variable. This results in a large amount of data that must be manipulated before further assessment can be completed. Further, the cellular model must be both reproducible and consistent (William J Buchser, Thomas C Laskow).

This high content screen was conducted with medium throughput rather than high throughput, providing evidence that a large-scale chemical screen can be conducted using affordable machinery and technical skill, though the overall pipeline may be slowed due to the smaller number of experiments that can be conducted at any given time. TIBCO Spotfire, a third-party analysis program, helped in the analysis of molecules that directionally regulate LC3 localization in the nucleus.

Chemical Validation and Normalization

To ensure the validity of the effects of the compounds, a correlation analysis was run between the assay plates and chemical source plate. Every compound was tested for correlation among two assay plates; high correlation was a strong indicator of accuracy. Plate effects were controlled for during analysis by rotating one of the two assay plates 180 degrees, overlaid on the other plate. In doing so, compounds were no longer aligned and should have had no correlation; any observed correlation was due to plate effects (**Supplemental Figure 2**). Using these control methods, we determined that obvious compound effect correlations existed among the data, and there were no observable plate effects. Covariance analysis provided insight into the variables that were most effected by compounds; notably, cytoplasmic LC3, nuclear LC3, nuclear area, and nuclear holes per nuclei were the four most correlated parameters.

Cell Culture and Transfection

Human cancer cell lines from ATCC (Manassas, VA) were used: 786-0 (CRL1932), CAKI-1 (HTB46), RCC4 (CVCL0498), pancreatic cell line PANC-1 (CRL1469), and human bladder cancer cell line T-24 (HTB-4). Cells were cultured in DMEM (Thermofisher 11995-065) supplemented with FBS (Thermofisher 26140079) and PenStrep (Thermofisher 15140-122) in a humidified incubator at 37°C with 5% CO_2. Cells were seeded in 96-well plates at 3,000 cells per well in 100µL of supplemented media. Plates were incubated at 37°C for 24 hours prior to manipulation.

Pre-designed SureSilencing™ short hairpin RNA (shRNA) plasmids from SABioscience (Frederick, MD) were used in order to target specific mRNA of importin β1 (KPNB1), importin 7 (IPO7), importin 8 (IPO8), and a scrambled negative control (Roggero et al.). For the time lapse experiments, we used the RFP-GFP-LC3B plasmid (Kimura, Noda, and Yoshimori) (gift

from Earl Godfrey). At 70% confluency, we transfected cells with shRNA plasmids or the RFP-GFP-LC3B plasmid using Lipofectamine 2000 (Thermofisher 11668-027) and the manufacturer's protocol. Ten hours after transfection, media was replaced and the cells were treated with the chemical compounds. After three hours, the compounds were rinsed out with fresh media, and the cells were incubated for 24 hours at 37°C.

Immunofluorescence

Following treatment and incubation, cells were fixed with 3.2% paraformaldahyde (ThermoFisher) in PBS. Plates were blocked and permeabilized in one step using bovine serum albumin (BSA) and 0.1% Triton X-100 in PBS at room temperature for 1 hour (both from Sigma-Aldrich). Antibodies were diluted in a blocking mixture consisting of a 1:1 ratio of PBS and BSA. Nuclear material was stained with Hoechst (ThermoFisher, H3570) at a 1:5000 dilution and endogenous LC3 was tagged with an LC3B/MAP1LC3B primary antibody (ThermoFisher, L10382) used at a dilution of 1:500 for 72 hours at 4°C. After incubation, the primary antibody was rinsed three times with PBS then Alexa Fluor 546-tagged goat anti-rabbit IgG secondary antibody (ThermoFisher, A-11035) was add at a 1:1250 dilution and incubated for 1 hour before a final 3x rinse with PBS.

Microscopy

Endpoint experiments were visualized using a Nikon inverted epifluorescence microscope. A 40x DIC objective was used with the DAPI (400-800 msec exposure) and TRITC (800-1600 msec exposure) filters. Microscopy was semi-automated such that four different images were acquired in each well (using *multi-point*) and the focal plane for each well was determined by eye (**Supplemental Figure 3**).

For confocal microscopy, cells were cultured on glass coverslips (#1.5), treated for a period of 4 hours, and subsequently fixed and stained after 24 hours. Coverslips were inverted and mounted onto glass slides using Fluoromount (Sigma-Aldrich). A Nikon confocal microscope was used to acquire Z-stacks at an average of 8-10 steps over a range of 6-9μM (top to bottom of the nucleus). The pinhole was set to 1.7 A.U., while laser power was held constant across samples.

For time-lapse experiments, 786-0 cells were transfected with an RFP-GFP-LC3 plasmid. After 8 hours, DMEM was replaced with FluoroBright DMEM (Thermofisher) and cells were treated with nucleophagy-modulating compounds. Temperature, CO_2, and humidity were kept constant in a live cell chamber. Images were captured via confocal microscopy at 20 minute intervals over 16 hours using a pinhole of 1.2 A.U. and 4x line averaging.

Image Analysis

Images were processed in *FIJI/ImageJ* (Schneider, Rasband, and Eliceiri). *ImageJ* was used to create maximum intensity projections of confocal z-stacks, z-slice views (dynamic reslice), and plot intensity profiles. Large 2x2 tiled images gathered from the inverted microscope were split into four by a script running in *ImageJ*. Open-source software *CellProfiler* was used for automated image analysis (Kamentsky et al.). The *CellProfiler* pipeline identified individual nuclei via Mixture of Gaussians (MoG) thresholding, which then allowed for analysis of intensity, localization, and prevalence of LC3 and nuclear material within the cell. The image-based flat files returned from *CellProfiler* were compiled, and *Spotfire DecisionSite* (Tibco Spotfire) was used to manually "quality control" the tracing by examining each of the traced wells for errors.

Images containing errors in tracing, those containing 2 cells or fewer per image, and those with obvious artifacts were excluded from analysis. The scripts for *ImageJ* and *CellProfiler* are included in the **Supplement**. Images that contained fewer than 3 cells per image, contained an error in tracing, or contained other artifacts were omitted from the overall analysis. When replicates from different plates (often from different cultures and days) were analyzed, they were first normalized so that the global mean of all the wells for all parameters studied were equal to 1 (by dividing by the global mean for each plate). To analyze the correlation between the two channels in cells, the *Coloc2* program in *ImageJ/FIJI* was used on two slices manually selected from a z-stack of confocal images.

Protein Analysis

Knockdown of importin β1, importin 7, and importin 8, compared to scrambled control shRNA, was validated by western blot by Dylan Zhang of Lizabeth Allison's lab as previously described (Roggero et al.). Briefly, 786-0 cells in 6-well plates were transfected with sets of four shRNA plasmids (SABioscience, Frederick, MD) and lysed 24 hours post-transfection. Antibodies were used with the following concentrations: anti-GAPDH (Santa Cruz Biotechnology Inc, Dallas, TX), 1:5000; anti-importin β1 (Santa Cruz), 1:2000; anti-importin 7 (Abcam, Cambridge, MA), 1:1000; anti-importin 8 (Abcam), 1:250. Seven independent replicates of each importin knockdown were completed from different cultures across distinct days.

Results

Compounds that Manipulate Nuclear Autophagic Puncta

Functional experiments analyzed 1600 chemical compounds for nuclear autophagic phenotypes (David Heo, Likhitha Kolla, 2017). Compounds were screened for modulation of nucleophagic activity, quantified by the average abundance of nuclear LC3 puncta. Of 1,309 compounds, two were able to induce distinct phenotypes. Of the 1600 compounds tested, 1309 passed quality control (QC), ranked by the replicate average Nuclear LC3, and 17 showed a notable increase in nuclear LC3 (**Figure 3**). 11 of these hits were considered significant after normalization, and one of the molecules was able to decrease nuclear LC3. Five compounds affected the number of holes per nuclei as well as the nuclear intesisity: four had a significant *increase* in holes (NSC60785, NSC126757, NSC279895 and NSC236246) and one had a significant *decrease* (DiHi).

A wide range of existing uses were found for some of the molecules that affected nuclear LC3. The two drugs described in this paper that affected an aneuploidy phenotype (NSC31762 and NSC279895) are notable in their potential to target relevant pathways. NSC31762 is structurally similar to thyroid hormone, and the phenyl moiety of NSC279895 may allosterically interact with the thryroid hormone receptor (THR) (**Figure 4**).

NSC367306, similar in structure to Benzoylurea, and NSC634396, similar to Benzothiazin, have been reported to have possible anti-cancer tendencies. Benzoylurea has previously been used as an insecticide, while Benzothiazin has reported anti-cancer activity. NSC636717 and NSC126757 are reported Shiga toxin inhibitors. NSC179818, related to chloroacridine, has been reported to have anti-inflammatory and anti-malarial effects.

NSC109128 is a sterol like compound that has been shown as an anti-viral in the setting of Hepatitis C.

The first of the molecules increased nuclear LC3 intensity; NSC31762, 2,6-**D**iiodo-4- [2-(1,3,3-**T**rimethylindol-2-ylidene) **E**thenyl] **P**henol (abbreviated ***DTEP***). Nuclear LC3 in cells exposed to DTEP at increasing concentrations (**Figure 5A**) had a significantly positive regression between DTEP concentration and LC3 enrichment within the nucleus (Linear regression, $p = 1.5 \times 10^{-5}$, F=58). DTEP is itself fluorescent at 590 nm, so may also be used as a tracer. The second compound decreased nuclear LC3 intensity; NSC279895, 1-(2,4-**Dihy**droxyphenyl) Heptane-1,2-Dione (abbreviated ***DIHI***). There was a significant decrease in nuclear LC3 intensity as DIHI concentration increased (**Figure 5B,** Linear regression p=0.0081, F=7.8). Seventy additional compounds affected at least one parameter measured, and half were selected for further experiments (Figure 10).

We asked whether DTEP's striking induction of nuclear punctae was conserved across cell types. Treatment with 20 μM DTEP produced a strong increase in nuclear LC3 across multiple cell lines, including renal lines 786-0, and CAKI-1, T-24 bladder cancer, as well as the pancreatic line PANC-1 (**Figure 5C**). In order to determine whether DTEP accelerated autophagy, we used the tandem pH-dependent RFP-GFP-LC3 reporter, in which acid sensitive GFP is quenched in the setting of the lysosome, leaving only RFP signals as an indicator of autophagic activity (Kimura, Noda, and Yoshimori). Treatment with vehicle (DMSO) or DIHI showed no significant change in GFP/RFP ratio over the course of an eight-hour period. A relative decrease in GFP, however, was observed in both the starvation treatment (PBS), as well as the 20μM DTEP treatment (**Figure 5D**). The loss of green fluorescence implied an increase in degradation of RFP-GFP-LC3 in the lysosome. Starvation with PBS induced a significant

increase in autophagic activity after 8 hours (t-test p=0.037), while the DTEP treatment caused a significant drop in the green/red ratio within a single hour (t-test $p=4.2x10^{-6}$). We conclude that DTEP and DIHI represent new chemical tools to modulate LC3 localization and autophagic flux.

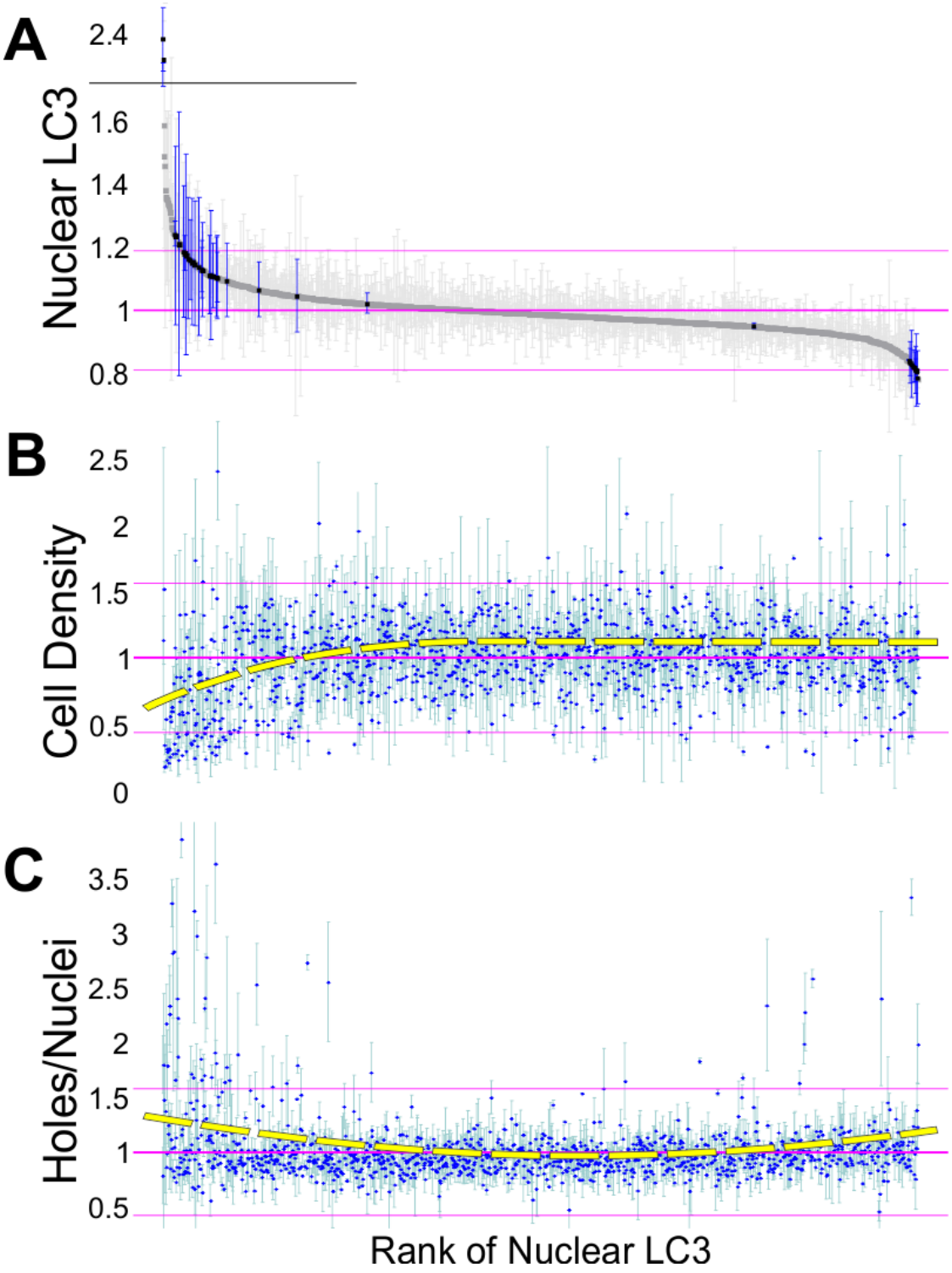

Figure 3. 1600-Compound Screening Results. From the initial 1600 compounds, 1309 passed quality control (QC). These hits were ranked by nuclear LC3 of the average of two plates **A)** Plot of the ordered QCs against the average nuclear LC3 values. We specifically chose to further investigate compounds with Nuclear LC3 values two standard deviations above or below the overall mean (indicated by the thick pink line). **B**) Ranked QCs were plotted against average cell densities (y) at point of fixation as an indicator of cell viability. Compounds with low cell

densities were considered toxic and omitted from the secondary assay. **C)** Holes per nuclei. Each coordinate represents the average parametric value of two experimental replicates for a QC, bars standard deviation

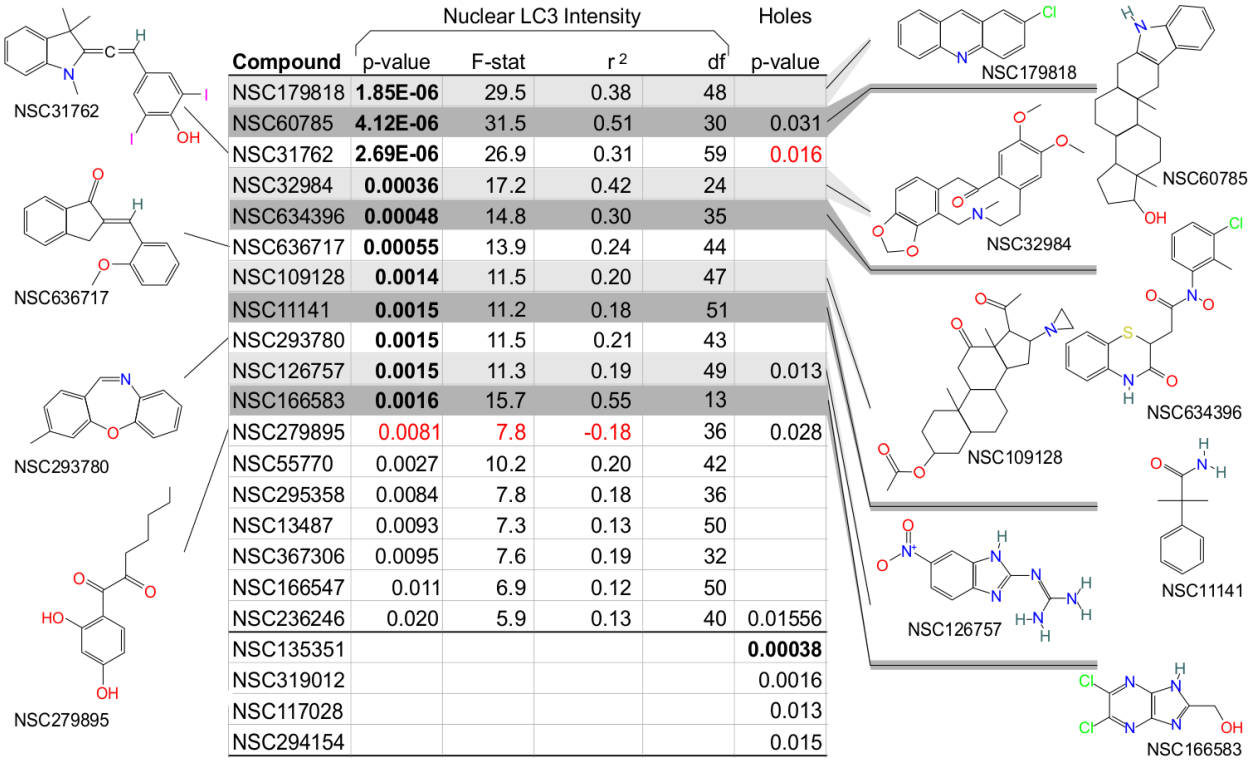

	Nuclear LC3 Intensity				Holes
Compound	p-value	F-stat	r^2	df	p-value
NSC179818	**1.85E-06**	29.5	0.38	48	
NSC60785	**4.12E-06**	31.5	0.51	30	0.031
NSC31762	**2.69E-06**	26.9	0.31	59	0.016
NSC32984	**0.00036**	17.2	0.42	24	
NSC634396	**0.00048**	14.8	0.30	35	
NSC636717	**0.00055**	13.9	0.24	44	
NSC109128	**0.0014**	11.5	0.20	47	
NSC11141	**0.0015**	11.2	0.18	51	
NSC293780	**0.0015**	11.5	0.21	43	
NSC126757	**0.0015**	11.3	0.19	49	0.013
NSC166583	**0.0016**	15.7	0.55	13	
NSC279895	0.0081	7.8	-0.18	36	0.028
NSC55770	0.0027	10.2	0.20	42	
NSC295358	0.0084	7.8	0.18	36	
NSC13487	0.0093	7.3	0.13	50	
NSC367306	0.0095	7.6	0.19	32	
NSC166547	0.011	6.9	0.12	50	
NSC236246	0.020	5.9	0.13	40	0.01556
NSC135351					**0.00038**
NSC319012					0.0016
NSC117028					0.013
NSC294154					0.015

Figure 4. Results from Secondary Screen. Stats for nuclear LC3 intensities and nuclear holes. Bolded p-values were still significant after correcting for multiple comparisons by Benjamini Hochberg. Red values represent a decreasing correlation while black values represent increasing correlations. Empty cells show lack of significance. Select compound morphologies are also shown.

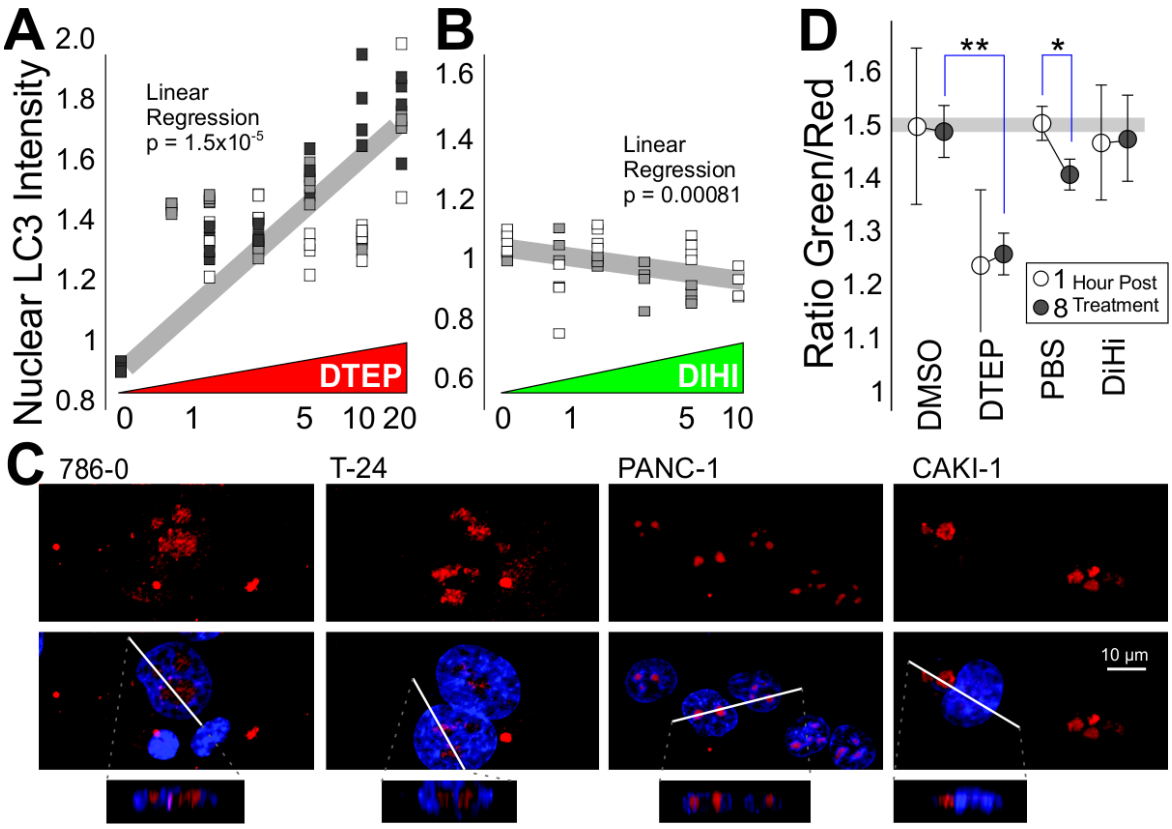

Figure 5. Compounds that Enhance and Inhibit LC3 Nuclear Puncta. A) Increasing concentrations (µM) of the compound DTEP resulted in a significant increase in nuclear LC3 compared to a DMSO control (Linear regression, $p=1.5x10^{-5}$). B) Increasing concentrations of the compound DIHI results in a significant decrease in nuclear LC3 intensity (p=0.0081). Markers represent well average, shadings indicate different biological replicates. C) Nucleophagy induced by *DTEP* in renal clear cell carcinomas (786-0, CAKI-1), T-24 bladder cancer, and pancreatic carcinoma PANC-1. LC3 (red) was found enriched within the nucleus (marked by DNA in blue). D) Cells transfected with a tandem RFP-GFP-LC3 sensor were monitored for autophagic activity over the course of eight hours. Markers show average ratio of green/red fluorescence with standard deviation between cells. Starvation (PBS) results in an increase in red signal (LC3 in the autolysosome, p = 0.037). Cells treated with 10 µM compound DTEP exhibit a significant increase in autophagy, especially eight hours after treatment (p = 0.00011).

Nuclear Autophagic Puncta Represent a Physiologic Intra-Nuclear Process

Previous examination of the autophagic signature of a number of cancer cell lines revealed that renal and pancreatic cells in particular were more likely to reveal nuclear LC3 puncta under both normal and stress conditions, justifying their use in these experiments

(Buchser et al.). While a fraction of control cells possess nuclear autophagic puncta, it is a relatively rare occurrence (**Figure 6A** black bars). DTEP's ability to induce nuclear puncta was analyzed in both 786-0 cells and PANC-1 over several biological replicates. DTEP increased the fraction of cells with nuclear LC3 by ~50% (% of cells with average nuclear LC3 intensity above DMSO control levels, **Figure 6A** gray bars, t-test, $p < 0.0001$).

We next asked how this chemical-induced phenotype compared to other autophagy-related phenotypes. 786-0 human renal cells were exposed to drug solvent (DMSO), macro-autophagy was induced using hydroxychloroquine (HCQ), and nuclear puncta were invoked using DTEP (as above). Confocal microscopy confirmed little to no LC3 in the cytoplasm or in the nucleus of most control cells (**Figure 6B**). When treated with HCQ, cells exhibit nonspecific macroautophagy that is most notably extra-nuclear (**Figure 6C**). There is little to no association between nuclear DNA intensity and LC3 intensity within the nucleus; most LC3 remains in the cytoplasm, as is seen both in the line scan and in the z-stack. When cells were treated with DTEP, prominent nuclear LC3 puncta appeared (**Figure 6D**). In the representative cell shown, LC3 & DTEP were localized to regions of low DNA density, which are referred to as "nuclear holes."

Presence of LC3 within the nucleus (not above or below) was confirmed using multi-step z-stack confocal microscopy. To determine whether the localization of the LC3 within the nucleus was consistent in the DTEP condition, a colocalization analysis was performed. Twenty-five representative images from biological replicates across three cell lines were analyzed. Individual nuclei were analyzed by confocal slice, and the correlation between LC3 and DNA was slightly lower in DTEP-treated cells than control (**Figure 6E**; t-test, $p = 0.048$). The variation between cells, however, was high, indicating that colocalization between these

nuclear holes and LC3 puncta may depend on the state of nucleophagic flux or other factors.

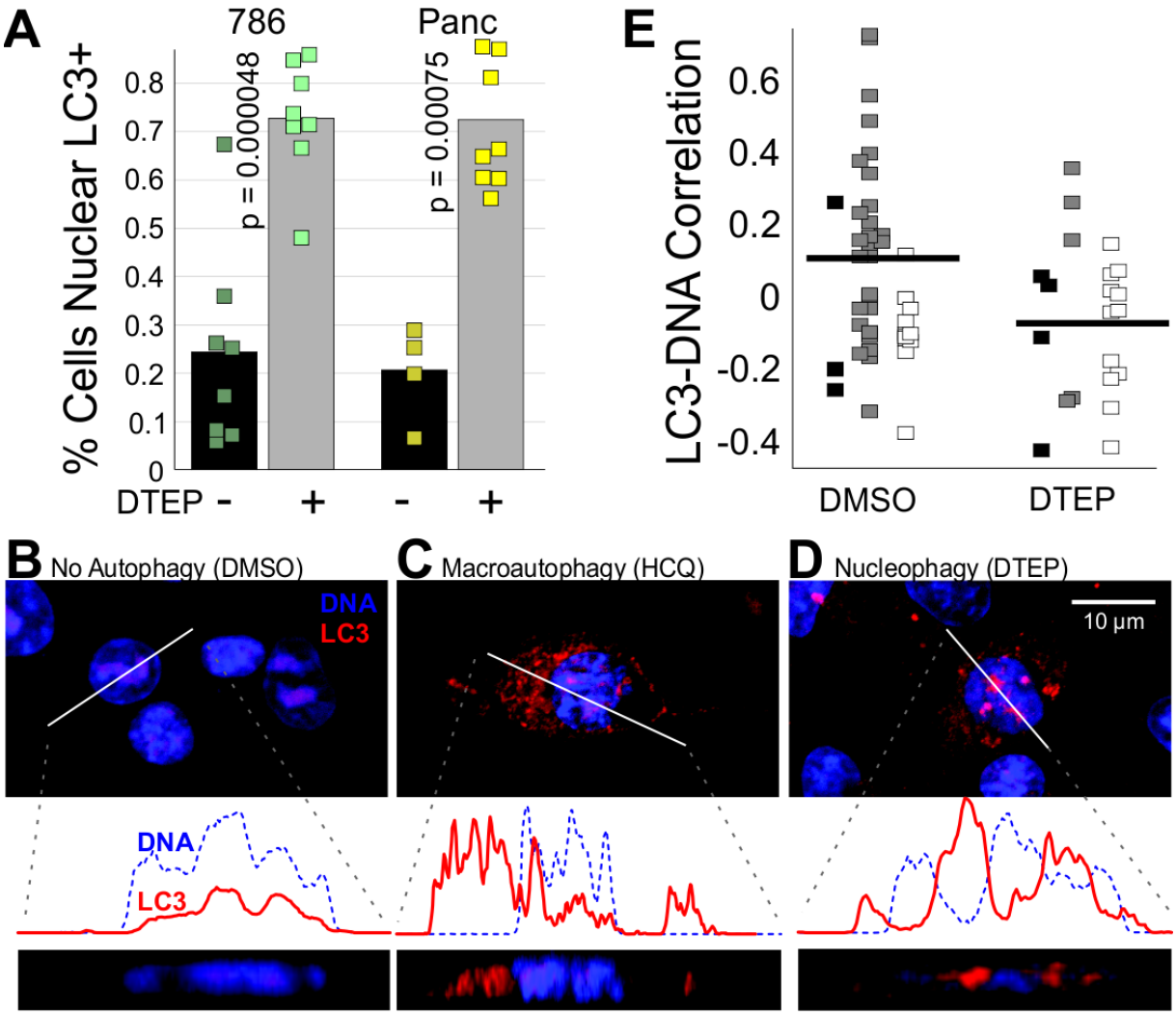

Figure 6. LC3 Nuclear-Autophagic Puncta are Phenotypically Distinct from Macro-autophagic Puncta. A) Markers show % of cells above background levels of nuclear autophagic puncta (4 biological replicates each). Bars demonstrate the average % cells per condition. The presence of DTEP significantly increases the percentage of cells that are positive for nuclear LC3 between both pancreatic and renal cell lines ($p < 0.001$, t-test of biologically independent replicates). **B-D** Upper panels are confocal slices on 786-0 cells. A line plot (generated based on the solid white line in the upper panels) indicates topographical association between DNA (blue) and LC3 (red). Below the line plot, a scale-matched depth reconstruction (z-stack) is shown. **B**) 786-0 cells treated with DMSO (vehicle) show low autophagic activity and weak topographical association. **C**) Cells treated with hydroxychloroquine (HCQ) have classic perinuclear localization of LC3. **D**) Treatment with the compound DTEP results in higher concentrations of LC3 inside the nucleus. Line scans show the anti-correlated nature of the DNA and LC3 (with LC3 localized to low-DNA "nuclear holes"). **E**) Nuclear LC3 puncta have variable amounts of colocalization with nuclear DNA ($p = 0.048$, dots represent the LC3-DNA pixel-pixel based Pearson's correlation of individual cells analyzed from 3 different cell lines; white: RCC4, gray: 786-9, black: CAKI-1).

Loss of Importins Induce Nuclear LC3 Localization

Our hypothesis that disrupting importin-dependent nuclear transport may induce nuclear stress and enhance nuclear autophagy was tested in the setting of knockdown of nuclear importins β1, 7 and 8. LC3 intensity within the nucleus was measured and compared to a scrambled shRNA control. Nuclear LC3 intensity significantly increased among importin β1, 7 and 8 knockdown cells compared with scrambled shRNA or untreated controls (**Figure 7A**, 2 wells each across 4 biologically independent replicates. ANOVA $p=0.000141$, $f=6.91$, post t-test $p = 0.00045$, $p = 0.014$, $p = 0.016$ respectively). These results suggest importins β1, 7, and 8 don't directly affect LC3 nuclear localization. Instead, the loss of importin-mediated nuclear transport may have triggered nuclear stress and subsequent nucleophagy. Knockdown efficiency was confirmed via western blot (**Figure 7B**).

Confocal microscopy determined whether the localization of LC3 was juxta-nuclear or intra-nuclear after importin knockdown (**Figure 7C**). Importin 7 knockdown resulted in prominent intra-nuclear localization of LC3 whereas Importin 8 knockdown had both intra- and resulted in more juxta-nuclear LC3.

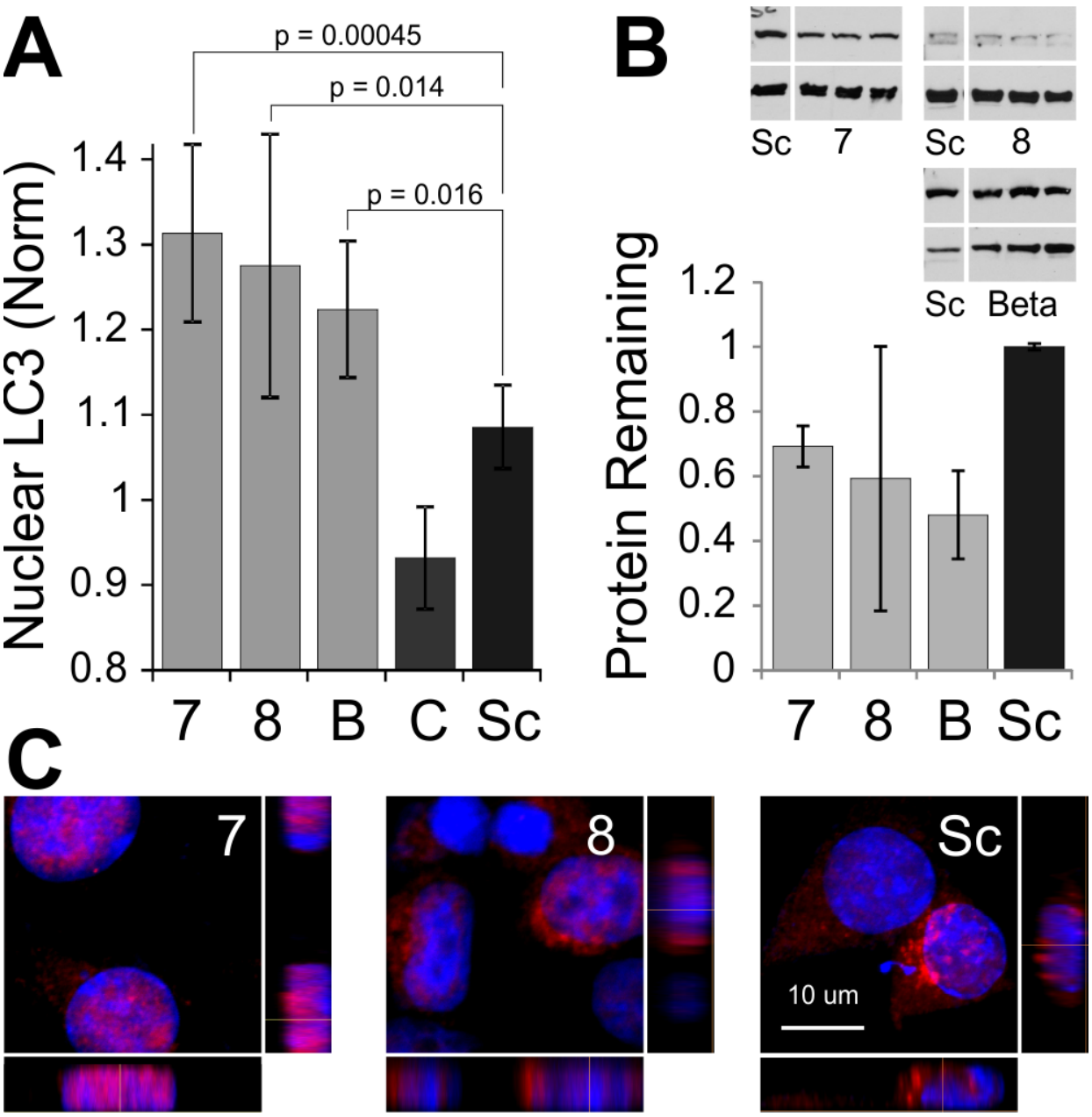

Figure 7. Knockdown of Several Importins Leads to Heightened Nuclear LC3 Accumulation. A) Average Nuclear LC3 intensity of 786-0 cells after knockdown of importins 7, 8 and β1, compared with untreated control and scrambled (Sc) shRNA. Error bars show standard deviation. **B**) Western blots (importins in upper bands and GAPDH in lower bands) and densitometric quantifications of knocked down importin 7, 8, and β1 when compared to a scrambled shRNA (average and standard deviation of 7 biological replicates). **C**) Micrographs show a maximum projection and two reconstructed "side views" of 786-0 renal cells transfected with shRNAs against importin 7, 8 or scrambled shRNAs. Cells were stained for LC3 (red) and DNA (blue). Importin 7 knockdown cells have the clearest intra-nuclear puncta (especially evident when viewed from the side), whereas importin 8 and Sc have both cytosolic and nuclear LC3 distribution.

Modulating Nucleophagy Can Revert an Aneuploidy Phenotype

To determine the functional consequences of these nuclear autophagic puncta, the two new nucleophagy tuning tools, DTEP and DIHI, were used in an applied physiological process associated with nuclear damage. Similar to previous studies (Dou et al.), we aimed to induce aneuploidy by introducing nuclear stress and triggering senescence. Two aneuploidogens, docetaxel and nocodazole, were used to halt normal cell division resulting in subsequent aneuploidy and oncogenic stress (**Figure 8**). 786-0 renal cells were exposed to a gradient of docetaxel (up to 3.2 µg/mL) to chemically induce aneuploidy (Hernández-Vargas, Palacios, and Moreno-Bueno) (**Figure 9A**). As the concentration of docetaxel increased, the cell density decreased, indicating either cell death or reduced cell division (Linear regression, $p=1.02x10^{-5}$, f=44.8). Furthermore, the average nuclear area increased ($p=1.78x10^{-5}$), likely indicating senescence. A representative image of an induced aneuploidy nuclear phenotype is shown in the middle panel of **Figure 9G**.

After optimizing induction of aneuploidy, we asked whether DTEP or DIHI could mitigate the effects of docetaxel. 786-0 renal cells were treated with 0.8 µg/mL of docetaxel for three hours and then subsequently exposed to a gradient of DTEP (up to 1µM **Figure 9B**). In the presence of an aneuploidogen induced phenotype, an increased concentration of DTEP resulted in a nuclear LC3 increase (bottom panel, p = 0.0047, f=16.7). DTEP was unable to interfere with the aneuploidy phenotype, and even minimally contributed to further cell density reduction (4B upper panels). On the other hand, DIHI was able to intercept the docetaxel-related mitotic effects (**Figure 9C**). 786-0 cells pre-treated with docetaxel and increasing concentrations of DIHI show a significant increase in cell density (4C upper panel, p=0.0042, f=12.0) and decrease

in nuclear area (middle panel, p=0.0043, f=11.9), indicating a reversion of the aneuploidogen-induced nuclear phenotype. Representative images of nuclei after treatment with docetaxel and DIHI are also shown (**Figure 9G** bottom panel).

A second aneuploidogen, nocodazole, was used to induce G_2/M arrest by interfering with microtubule polymerization resulting in polyploidy. As the concentration of nocodazole was increased (up to 30 µg/mL), the cell density decreased while nuclear area increased (**Figure 9D**, linear regression density $p=2.9x10^{-5}$, f=39.2, area p=0.0067, f=10.4), indicating reduced cell division due to mitotic blockade. We then asked whether DTEP or DIHI were able to interfere with the effects of nocodazole by exposing 786-0 cells to 15µg/mL nocodazole and a subsequent DTEP gradient. DTEP concentration and nuclear LC3 were found to have a positive relationship as seen in previous experiments, but DTEP was unable to reverse nocodazole's phenotypic effects, possibly making them more pronounced (**Figure 9E)**. When DIHI was added in the presence of 15 µg/mL of nocodazole, there was no *significant* change in LC3, area, or cell density. We conclude DIHI, which we showed to inhibit nuclear autophagic puncta, protects the cells from a *docetaxel*-induced aneuploidy phenotype.

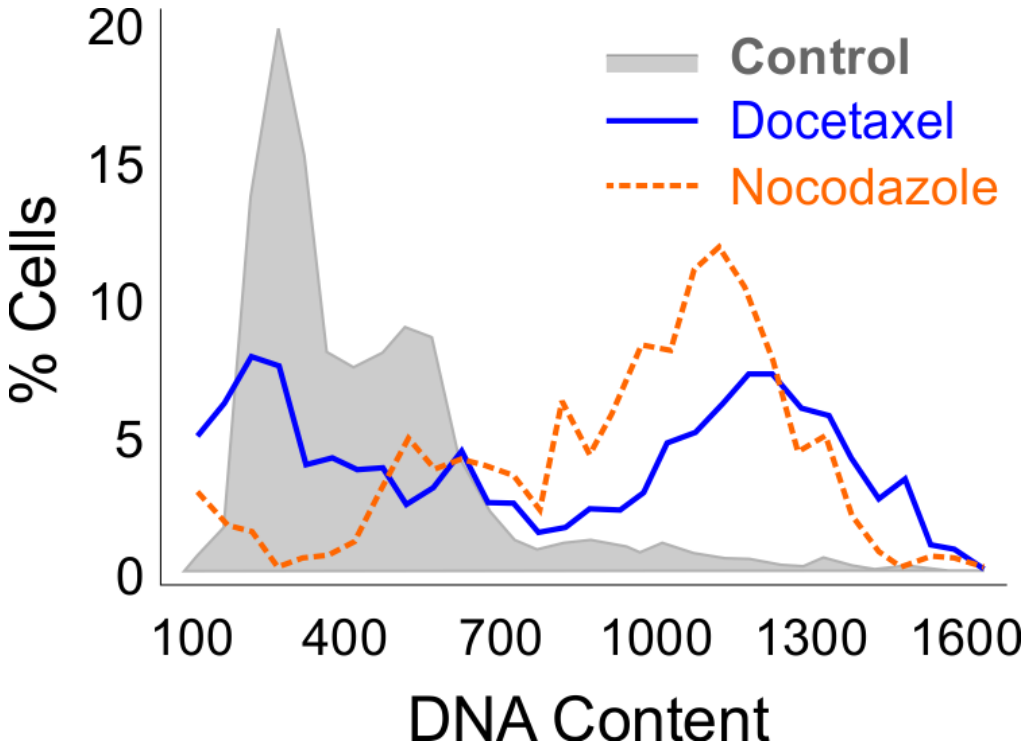

Figure 8. **Chemical induction of aneuploidy**. Histograms showing the distribution of individual cells on a scale of integrated blue fluorescence intensity, representative of DNA content. Control cells (gray shaded region) have a primarily unimodal population distribution with most cells in the low DNA content range of 400-700 MFU (mostly diploid nuclei). Nocadozole treated cells (orange dotted line) show a bimodal distribution with more cells in the 800-1400 MFU range, indicating polyploidy. Docetaxel treated cells (blue solid line) appear to show a multimodal distribution of cells with abnormal, non-multiplicative DNA content, likely illustrating the induction of aneuploidy.

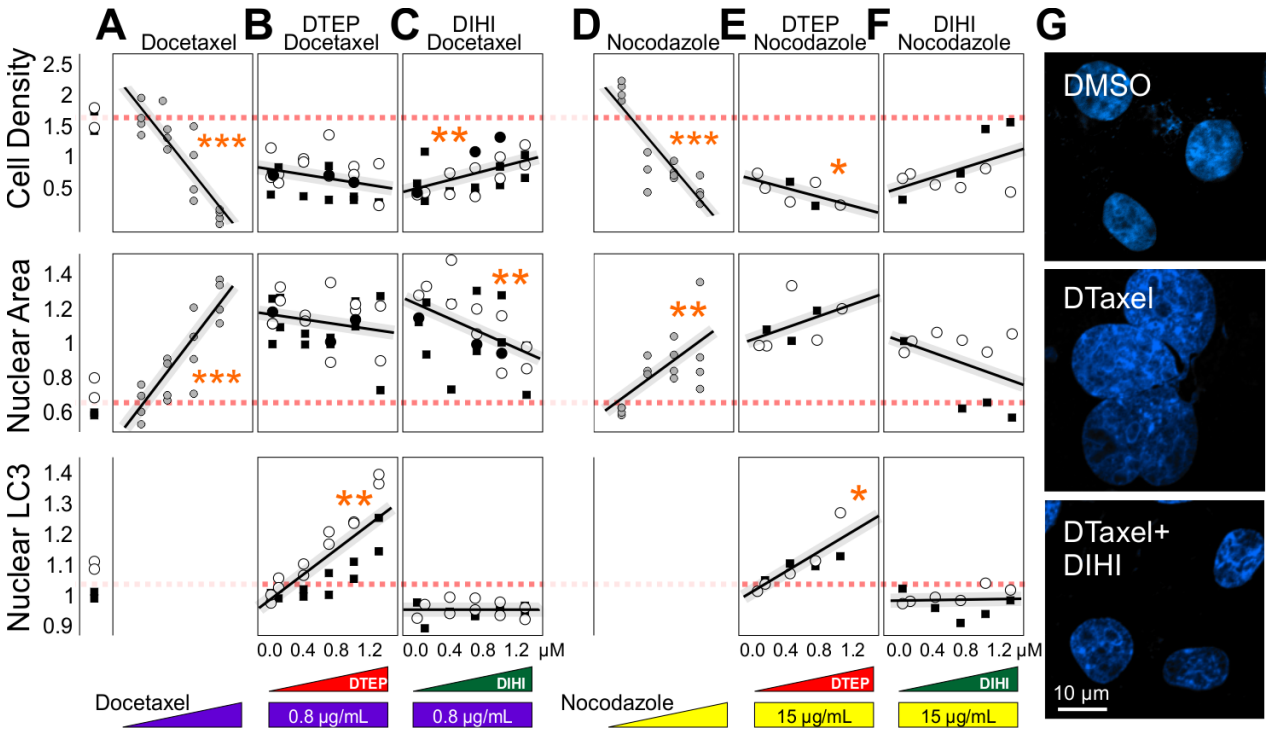

Figure 9. Compound DIHI can Revert the Phenotype in Docetaxel- and Nocodazole-treated cells. A-F) 786-0 responses after exposure to various treatments. Upper panels show cell density, middle panels show nuclear area, and bottom panels show nuclear LC3 intensity. Markers represent normalized well averages from independent experiments (indicated by different marker types). Control levels of cell density, nuclear area, and nuclear LC3 are indicated by the red dashed lines traversing the panels. **A-C**) Cells treated with docetaxel, **D-F**) cells treated with nocodazole. **A)** Increasing docetaxel dose reduces cell density, and increases nuclear area increases (asterisks indicate significance in a linear regression). In the presence of background docetaxel, DTEP (**B**) or DIHI (**C**) were added in increasing doses. **D)** A nocodazole gradient lowers cell density and increases nuclear area through mitotic blockade. Increasing doses of the compounds DTEP (**E**) and DIHI (**F**). **G**) Representative confocal images of 786-0 renal cells exposed to DMSO (top), docetaxel 0.8 µg/mL (DT, middle), or docetaxel and 15 µM DIHI (bottom).

Discussion

While some studies have documented nuclear autophagy as a cellular phenomenon, none have been able to specifically manipulate the process. We have shown here that nucleophagy is a phenotypically specific form of autophagy distinct from macroautophagy and may be implicated in the survival of cells under nuclear stress. Additionally, we have utilized two recently-identified small molecules (DTEP, DIHI) to regulate the amount of LC3 that is present within the nucleus. We attempted to elucidate the relationship between nuclear stress and nucleophagy by knocking down components of the nuclear import machinery. As expected from previous studies (Drake, Kang, and Kenworthy), nuclear importins 7, 8, and β1 do not appear to play a role in LC3 nuclear entry. Instead, the knockdown of these importins led to nuclear stress which induced nuclear autophagic puncta. The presence of nucleophagy across multiple cell lines suggests that the process is not an artifact confined to a specific subset of cells (Buckingham et al.), rather, a distinct stress response pathway that is likely conserved. Nucleophagy is associated with an increase in LC3 found in nuclear holes within the nucleus. In the setting of aneuploidy, we found that treatment with DIHI, a potential inhibitor of nucleophagy, results in the blockage of senescence and an increase in cell numbers (thus undoing the effects of docetaxel).

Nuclear-associated autophagy likely encompasses a collection of varied cellular mechanisms with diverse functions that may span the activation of senescence, disposal of micronuclei, and perhaps even removal incongruous strands of DNA (Dou et al.). Our ability to control and disrupt these processes is critical in order to understand their function and mechanism, while simultaneously leveraging the process for therapeutic reasons. We hypothesize, in accordance with (Dou et al.), DTEP may cause an increase in lamin-degrading nucleophagy specifically under the presence of nuclear stress, resulting in the high occurrence of

nuclear autophagic puncta observed. Furthermore, (Dou et al. 2015) concludes that an inhibition of the nuclear lamina degradation via the knockdown of the basal autophagy gene Atg7 decreases the rate of degradation of nuclear lamina and prevents the induction of protective senescence. We have discovered a chemical tool, DIHI, which may also inhibit this lamin-degrading nucleophagy, thus preserving the nucleus, allowing for continued cell division. This inhibition allows for an increased potential for oncogenic transformation and an increased risk of cancer (Dou et al.). An alternative hypothesis is that DTEP could be disrupting the completion of nucleophagy, causing a buildup of LC3 within the nucleus without subsequently increasing autophagic flux. Based on our measurements of flux with RFP-LC3-GFP, this seems unlikely. Future studies utilizing these tools will allow us and others to reveal the complex mechanisms underlying nucleophagy.

Further work is being done to provide additional evidence characterizing nucleophagy and the effects of compounds DTEP and DIHI. Biochemical assays, including protein abundance analysis of LC3B, importins 7 and 8, as well as Lamin B1 will allow us to determine both potential pathways our chemicals target as well as some of the mechanisms of LC3 transport during nucleophagy. Additional experiments are also in progress to confirm the legitimacy of the aneuploidy phenotype through heterokaryon assays and G-banding.

Now that nucleophagy has been generally characterized, there are three important directions in which further research and investigation may continue. First, the identity of the sensors and signaling networks that activate nucleophagy are still unknown, and substrate targeting are not understood. The egress of nuclear material via nucleophagy has now been described in more detail (Dou et al.), but the mechanism by which the autophagic machinery enters the nucleus is unclear. Previous studies (Drake, Kang, and Kenworthy) suggest LC3

enters the nucleus via passive diffusion, but this result is unsatisfying. In the setting of importin knockdown (IPO8 specifically), some LC3 that might have other otherwise traversed the nuclear envelope was unable to enter the nucleus, implying a partial mode of specific transport by IPO8. More studies will have to carefully explore these mechanisms.

Our second goal queries nucleophagy's role in disease, including cancer and neurodegenerative diseases such as amyotrophic lateral sclerosis (ALS) and Alzheimer's. Various mutations, including the ALS *C9orf72* mutant, are known to result in nuclear stress due to RAN proteotoxic aggregates and, perhaps more interestingly, the buildup of antisense RNA foci within the nucleus (Hayes and Rothstein). The implication of nucleophagy as a potential disposal system for these mis-incorporated products may be critical for the survival of cells in the onset of these diseases. *C9orf72* mutants are known to have irregularities in the structure and stability of the nuclear envelope directly related to the length of the repeat, which ultimately leads to degeneration of neuronal tissue and failure of the nuclear pore to allow effective nucleocytoplasmic transport (Freibaum et al.). Given that recent findings suggest the direct connection between *C9orf72* and an increase in autophagic flux (Yang et al.), the next logical step is to investigate the presence and potential role of nucleophagy in cell survival in the setting of ALS and familial frontotemporal dementia (FTD).

Finally, more research may reveal the prevalence of nucleophagy in the tumor microenvironment. Tandem to the role of *C9orf72* in autophagy regulation is the influence of heterotypic interactions of the tumor microenvironment. Dysfunctional autophagy is known to induce tumorigenesis, making this connect particularly interesting. Previous research has highlighted the role of immune cells (human peripheral blood lymphocytes) in inducing autophagy to promote tumor cell survival and proliferation (Buchser et al.). Despite these

advances, many questions still remain, including how the surrounding stromal, immune, and endothelial cells can affect the specificity and magnitude of *nucleophagic* flux in tumor cells. Furthermore, we would like to ask how this cell mediated behavior can regulate crosstalk within the physiological environment to activate and modulate pathways, respond to metabolic stress, and maintain homeostasis. Ultimately, looking at these heterotypic orchestrations will give better intuition for therapeutic targets that modulate both autophagy and the tumor microenvironment to hinder cancer cell progression and metastasis.

Supplemental Figures

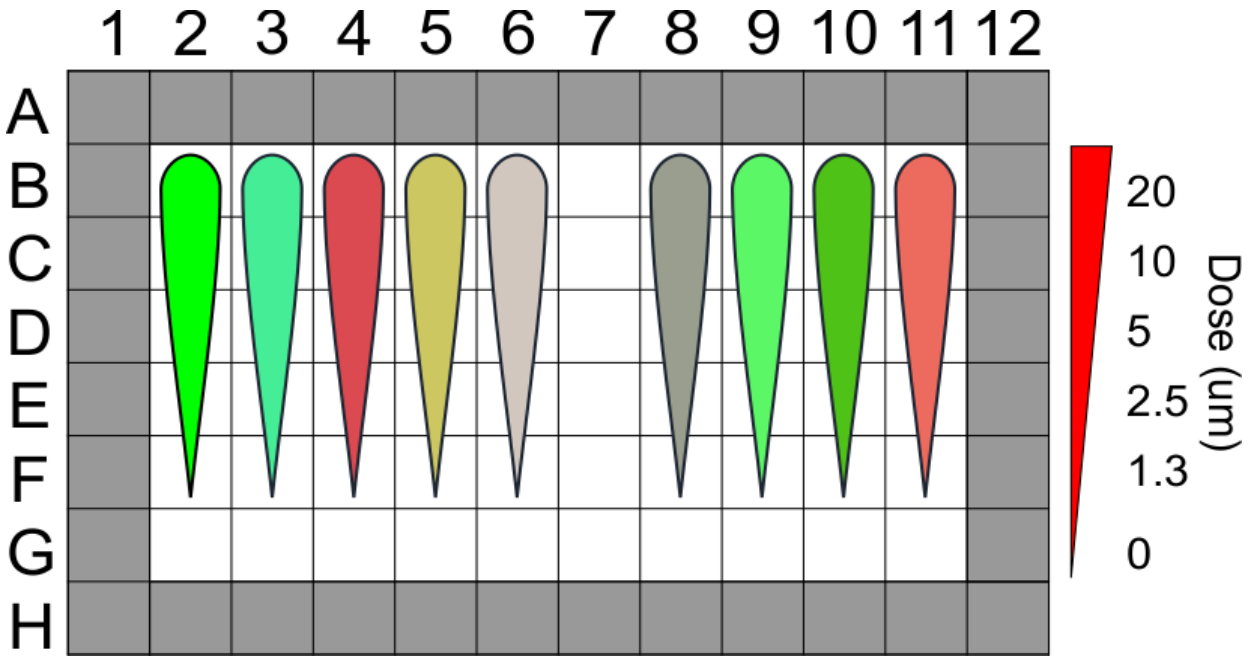

Supplemental Figure 1. Plate Layout of Secondary Assay. Perimeter wells left untreated, with only media and the diluent (10% DMSO and 90% PBS). Individual compounds of interest were added in decreasing doses down the columns, indicated by the separate colored gradients in the schematic. The downward gradients represent a serial dilution of the drug from 20µM to 1.25µM, with the last row (G) left untreated (0µM) as a control.

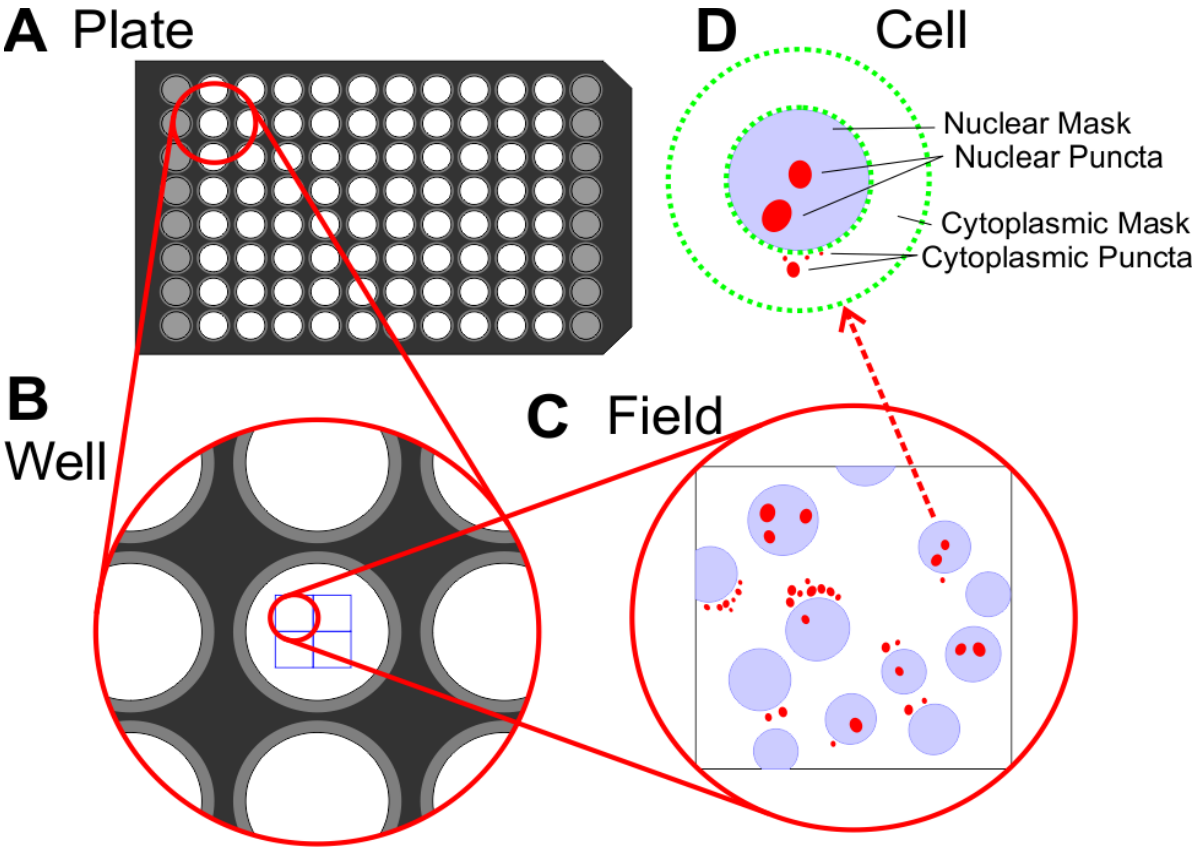

Supplemental Figure 2. Assay Hierarchy and Tracing. A) 96-well plates were used throughout the entire screening process B) A consistent automated 2x2 imaging pattern was established prior to imaging to capture four separate images per well, later stitched together to get a complete image of the well via NIS-Elements. C) Images were split into separate fields via FIJI/ImageJ software, then rerouted to CellProfiler to analyze/obtain D) cytometric data on the number of LC3 puncta in the nuclei and cytoplasm, nuclear and cytoplasmic LC3 levels, nuclear and cytoplasmic masks.

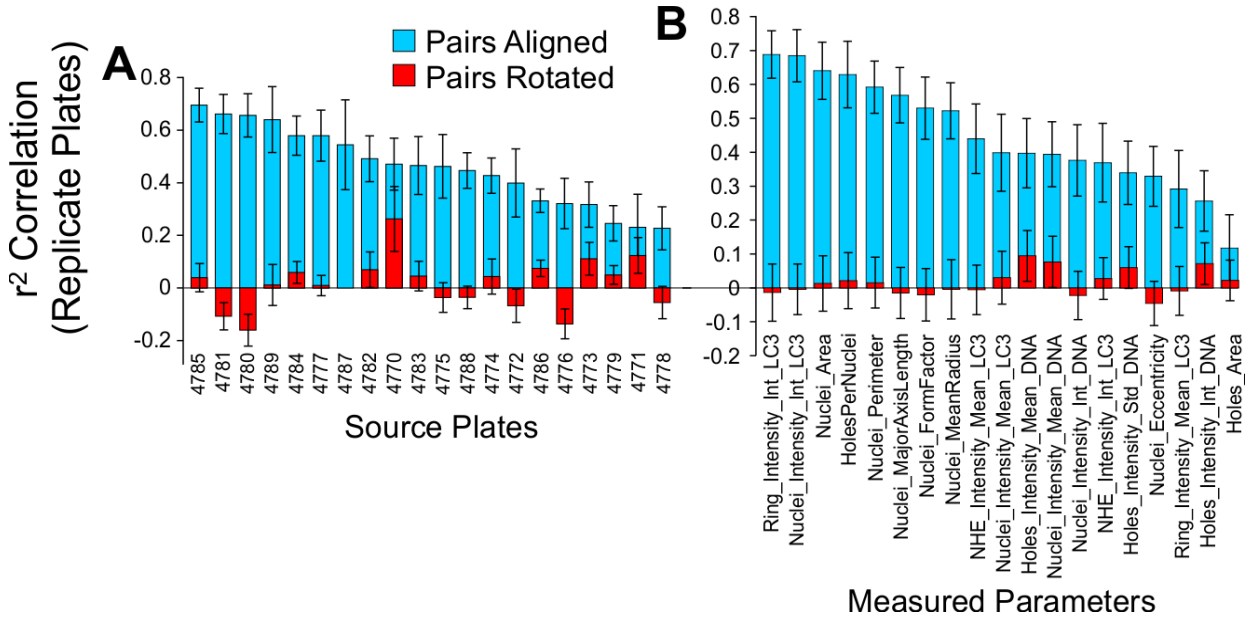

Supplemental Figure 3. Correlation analysis of plates and parameter. Each pair of plates from the primary screen was analyzed by comparing it to its replicate directly or by rotating 180 degrees and comparing. Each plate was screened twice with separate cell passages. **A.** Individual Plate IDs are compared well-to-well with their replicate. The displayed value is the average of all the measured parameters (listed in **B**), with standard deviation. **B.** Individual measured parameters (ranked by best to worst) - x-axes are comparable to A respectively.

References

Akinduro, Olufolake et al. "Constitutive Autophagy and Nucleophagy during Epidermal Differentiation." *The Journal of investigative dermatology* (2016): 1–11. Web.

Amaravadi, Ravi K et al. "Autophagy Inhibition Enhances Therapy-Induced Apoptosis in a Myc -Induced Model of Lymphoma." 117.2 (2007): n. pag. Web.

Biamonti, Giuseppe, and Claire Vourc'h. "Nuclear Stress Bodies." *Cold Spring Harbor perspectives in biology* 2.6 (2010): 1–12. Web.

Buchser, William J et al. "Cell-Mediated Autophagy Promotes Cancer Cell Survival." *Cancer Research* 72.12 (2012): 2970–2979. Web.

Buckingham, Erin M et al. "Nuclear LC3-Positive Puncta in Stressed Cells Do Not Represent Autophagosomes." *BioTechniques* 57.5 (2014): 241–4. Web.

Carneiro, Leticia A M, and Leonardo H Travassos. "The Interplay between NLRs and Autophagy in Immunity and Inflammation The Interplay between NLRs and Autophagy in Immunity and Inflammation." November 2013 (2017): n. pag. Web.

Codogno, P, and A J Meijer. "Autophagy and Signaling: Their Role in Cell Survival and Cell Death." *Cell Death and Differentiation* 12 (2005): 1509–1518. Web.

D'Angelo, Maximiliano A. et al. "Age-Dependent Deterioration of Nuclear Pore Complexes Causes a Loss of Nuclear Integrity in Postmitotic Cells." *Cell* 136.2 (2009): 284–295. Web.

Dou, Zhixun et al. "Autophagy Mediates Degradation of Nuclear Lamina." *Nature* 527.7576 (2015): 105–109. Web.

Drake, Kimberly R, Minchul Kang, and Anne K Kenworthy. "Nucleocytoplasmic Distribution and Dynamics of the Autophagosome Marker EGFP-LC3." *PloS one* 5.3 (2010): e9806. Web.

Freibaum, Brian D. et al. "GGGGCC Repeat Expansion in C9orf72 Compromises Nucleocytoplasmic Transport." *Nature* 525.7567 (2015): 129–33. Web.

Gomes, Ligia C., and Luca Scorrano. "Mitochondrial Morphology in Mitophagy and Macroautophagy." *Biochimica et Biophysica Acta (BBA) - Molecular Cell Research* 1833.1

(2013): 205–212. Web.

Hayes, Lindsey R., and Jeffrey D. Rothstein. "C9ORF72-ALS/FTD: Transgenic Mice Make a Come-BAC." *Neuron* 90.3 (2016): 427–431. Web.

Heo, David et al. *Pharmacologic Agents Targeting Manipulating Nucleophagy in Renal Cancer Cell Lines*. N.p., 2017. Print.

Hernández-Vargas, H, J Palacios, and G Moreno-Bueno. "Molecular Profiling of Docetaxel Cytotoxicity in Breast Cancer Cells: Uncoupling of Aberrant Mitosis and Apoptosis." *Oncogene* 26.20 (2007): 2902–13. Web.

Hirano, Makito et al. "ALADINI482S Causes Selective Failure of Nuclear Protein Import and Hypersensitivity to Oxidative Stress in Triple A Syndrome." *Proceedings of the National Academy of Sciences of the United States of America* 103 (2006): 2298–2303. Web.

Kamentsky, Lee et al. "Improved Structure, Function and Compatibility for Cellprofiler: Modular High-Throughput Image Analysis Software." *Bioinformatics* 27.8 (2011): 1179–1180. Web.

Kimura, Shunsuke, Takeshi Noda, and Tamotsu Yoshimori. "Dissection of the Autophagosome Maturation Process by a Novel Reporter Protein, Tandem Fluorescent-Tagged LC3." *Autophagy* 3.5 (2007): 452–460. Web.

Klionsky, Daniel J et al. "Guidelines for the Use and Interpretation of Assays for Monitoring Autophagy (3rd Edition)." *Autophagy* 12.1 (2016): 1–222. Web.

Kose, Shingo, Maiko Furuta, and Naoko Imamoto. "Hikeshi, a Nuclear Import Carrier for Hsp70s, Protects Cells from Heat Shock-Induced Nuclear Damage." *Cell* 149.3 (2012): 578–589. Web.

Kraft, Claudine, Fulvio Reggiori, and Matthias Peter. "Selective Types of Autophagy in Yeast." *Biochimica et Biophysica Acta - Molecular Cell Research* 1793.9 (2009): 1404–1412. Web.

Levine, Beth, and Daniel J. Klionsky. "Development by Self-Digestion: Molecular Mechanisms and Biological Functions of Autophagy." *Developmental Cell* 6.4 (2004): 463–477. Web.

Liang, X H et al. "Induction of Autophagy and Inhibition of Tumorigenesis by Beclin 1." *Nature* 402.6762 (1999): 672–676. Web.

Lipatova, Zhanna, and Nava Segev. “A Role for Macro-ER-Phagy in ER Quality Control.” (2015): 1–29. Web.

Mah, L-J, a El-Osta, and T C Karagiannis. “gammaH2AX: A Sensitive Molecular Marker of DNA Damage and Repair.” *Leukemia : official journal of the Leukemia Society of America, Leukemia Research Fund, U.K* 24.4 (2010): 679–686. Web.

Marquez, Rebecca T, and Liang Xu. “Bcl-2 : Beclin 1 Complex : Multiple , Mechanisms Regulating Autophagy / Apoptosis Toggle Switch.” 2.2 (2012): 214–221. Print.

Mathew, Robin et al. “Autophagy Suppresses Tumor Progression by Limiting Chromosomal Instability.” Baehrecke 2003 (2007): 1367–1381. Web.

Mijaljica, Dalibor, and Rodney J Devenish. “Nucleophagy at a Glance.” *Journal of cell science* 126.Pt 19 (2013): 4325–4330. Web.

Mijaljica, Dalibor, Mark Prescott, and Rodney J Devenish. “The Intricacy of Nuclear Membrane Dynamics during Nucleophagy.” *Nucleus* 1.3 (2010): 213–223. Web.

Mizushima, Noboru. “Autophagy : Process and Function.” (2007): 2861–2873. Web.

Mizushima, Noboru, and Tamotsu Yoshimori. “How to Interpret LC3 Immunoblotting.” *Autophagy* 3.6 (2007): 542–545. Web.

Park, Young-Eun et al. “Autophagic Degradation of Nuclear Components in Mammalian Cells.” *Autophagy* 5.6 (2009): 795–804. Print.

Roggero, Vincent R. et al. “Nuclear Import of the Thyroid Hormone Receptor α1 Is Mediated by Importin 7, Importin β1, and Adaptor Importin α1.” *Molecular and Cellular Endocrinology* 419 (2016): 185–197. Web.

Rogov, Vladimir et al. “Interactions between Autophagy Receptors and Ubiquitin-like Proteins Form the Molecular Basis for Selective Autophagy.” *Molecular Cell* 53.2 (2014): 167–178. Web.

Santaguida, Stefano et al. “Aneuploidy-Induced Cellular Stresses Limit Autophagic Degradation.” *Genes and Development* 29.19 (2015): 2010–2021. Web.

Schneider, Caroline a, Wayne S Rasband, and Kevin W Eliceiri. “NIH Image to ImageJ: 25 Years of Image Analysis.” *Nature Methods* 9.7 (2012): 671–675. Web.

Schuck, Sebastian, Ciara M Gallagher, and Peter Walter. "ER-Phagy Mediates Selective Degradation of Endoplasmic Reticulum Independently of the Core Autophagy Machinery." (2014): 4078–4088. Web.

Stewart, Murray. "Molecular Mechanism of the Nuclear Protein Import Cycle." *Nature reviews. Molecular cell biology* 8.3 (2007): 195–208. Web.

Torres, Eduardo M., Bret R. Williams, and Angelika Amon. "Aneuploidy: Cells Losing Their Balance." *Genetics* 2008: 737–746. Web.

Tsuboi, Shigeru. "Autophagy in Yeast Demonstrated with Proteinase-Deficient Mutants and Conditions for Its Induction." 119.2 (1992): 3–8. Print.

Ugolino, Janet et al. "Loss of C9orf72 Enhances Autophagic Activity via Deregulated mTOR and TFEB Signaling." *PLOS Genetics* 12.11 (2016): e1006443. Web.

William J Buchser, Thomas C Laskow, Philip J Pavlik. "Cell-Mediated Autophagy Promotes Cancer Cell Survival William." 72.12 (2013): 2970–2979. Web.

Wong, Alan S L, Zelda H Cheung, and Nancy Y Ip. "Molecular Machinery of Macroautophagy and Its Deregulation in Diseases." *Biochimica et biophysica acta* 1812.11 (2011): 1490–7. Web.

Xie, Zhiping, and Daniel J Klionsky. "Autophagosome Formation : Core Machinery and Adaptations." 9.10 (2007): n. pag. Print.

Yang, Mei et al. "C9ORF72/SMCR8-Containing Complex Regulates ULK1 and Plays a Dual Role in Autophagy." *Life Sciences* September (2016): 1–18. Web.

Yang, Zhifen, and Daniel J Klionsky. "Eaten Alive : A History of Macroautophagy." *Nature Publishing Group* 12.9 (2010): 814–822. Web.

Yorimitsu, Tomohiro et al. "Endoplasmic Reticulum Stress Triggers Autophagy *." 281.40 (2006): 30299–30304. Web.

Zhang, K et al. "The C9orf72 Repeat Expansion Disrupts Nucleocytoplasmic Transport." *Nature* 525.7567 (2015): 56–61. Web.